Agricultural and Forest Meteorology 377 (2026) 110951

Contents lists available at ScienceDirect

Agricultural and Forest Meteorology

journal homepage: www.elsevier.com/locate/agrformet

Understanding forest wind damage during mountain wave events: Insights from a case study in Norway

Peter Zubkov [a], Harold McInnes [b], Eirik Mikal Samuelsen [c], Kristina Blennow [d,e,*]

[a] Norwegian University of Life Sciences, P.O. Box 5003, NO-1432 Ås, Norway
[b] Norwegian Meteorological Institute, P.O. Box 43 Blindern, NO-0313 Oslo, Norway
[c] Norwegian Meteorological Institute, P.O. Box 6314 Langnes, NO-9293 Tromsø, Norway
[d] Department of Landscape Architecture, Planning, and Management, Swedish University of Agricultural Sciences, P.O. Box 190, S-234 22 Lomma, Sweden
[e] Department of Physical Geography and Ecosystem Science, Lund University, Sölvegatan 12, S-223 62 Lund, Sweden

ARTICLE INFO

Keywords:
Downslope windstorm
Forest windthrow
Turbulent airflow
Gravity waves

ABSTRACT

Forest wind damage models are typically based on the assumption that windstorm damage results from the interaction between horizontal wind forces and forest stand properties. In complex terrain, mountain waves caused by stably stratified air flowing over mountains can generate standing waves and severe downslope windstorms on the leeward side. Using the windstorm of 19 November 2021 in a mountain valley in southeastern Norway as a case study, we tested two hypotheses:

1. Forest stand properties do not significantly contribute to explaining forest damage during a mountain wave event.

2. Meteorological variables related to atmospheric stratification, turbulence, and non-horizontal airflow significantly contribute to explaining forest damage during a mountain wave event.

To test these hypotheses, we combined forest damage observations with a high-resolution numerical weather prediction model and Random Forest modeling. We used SHapley Additive exPlanations (SHAP) values to quantify the contributions of individual model features. Incorporating forest stand variables did not significantly improve predictive performance, whereas potential temperature gradient, vertical airflow velocity, and wind gust speed, capturing turbulence, did. SHAP analysis showed that although wind gust speed helped explain damage, its influence was secondary to that of potential temperature gradient, which had the strongest explanatory power. The model demonstrated good discriminative power between damage and no damage in the test set. Our findings underscore the limitations of conventional models reliant on horizontal wind speed, highlighting the need for high-resolution numerical weather prediction models that resolve three-dimensional flow in complex terrain, especially during mountain wave events.

1. Introduction

In 1950–2000, wind was a major natural disturbance agent in European forests, responsible for 53 % of the damage in terms of wood volume, followed by fire, bark beetles, and snow (Gardiner et al., 2010; Schelhaas et al., 2003). As reported in Patacca et al. (2023), the average forest damage caused by wind in 1950–2019 was 23 million m^3 y^{-1}, peaking at 48 and 38 million m^3 y^{-1} in the 1990s and 2000s, respectively. Windstorms cause a variety of negative impacts on forests, extending beyond reduced timber quality and value, to include increased harvesting costs, disruptions to timber supply chains, and secondary biotic damage, such as bark beetle outbreaks (Blennow and Persson, 2013; Hanewinkel and Peyron, 2013; Komonen et al., 2011; Økland and Berryman, 2004; Romagnoli et al., 2023; Schwarzbauer and Rauch, 2013).

Extreme winds in Northern Europe are mainly associated with extratropical cyclones during the winter months (Feser et al., 2015) and convective weather such as thunderstorms during summer (Pettit et al., 2021). In winter, climate warming-related changes in the intensity, frequency, or cyclone tracks of low-pressure systems, such as tropical cyclones transforming into increasingly more destructive extratropical cyclones (Cheung and Chu, 2023; Jung and Lackmann, 2023), could influence future windiness. In summer, changes in humidity caused by a warmer climate may alter the frequency and intensity of thunderstorms,

* Corresponding author.
E-mail address: kristina.blennow@slu.se (K. Blennow).

https://doi.org/10.1016/j.agrformet.2025.110951
Received 6 May 2025; Received in revised form 16 October 2025; Accepted 19 November 2025
Available online 24 November 2025

which are convective weather systems driven by atmospheric instability. While Patacca et al. (2023) found only a weak trend in wind disturbances over the past 70 years, an increased risk of wind damage associated with a warming climate cannot be ruled out. The effect of climate change on future windiness in northern Europe is considered uncertain (Gregow et al., 2020; Groenemeijer et al., 2016; Kjellström et al., 2018; Ruosteenoja et al., 2019). Feser et al. (2015) note that while the number of storms in northwestern Europe may remain unchanged, their intensities may increase. Despite the uncertainties surrounding future extratropical cyclone activity in Europe under changing climatic conditions (Intergovernmental Panel on Climate Change (IPCC), 2023), simulation studies suggest that forest vulnerability to wind damage may increase in a changing climate, even without intensification of wind speeds, if current management regimes remain unchanged (Blennow et al., 2010; Díaz-Yáñez et al., 2019; Ikonen et al., 2017; Venäläinen et al., 2004).

Over the years, research has provided valuable insight into the factors predisposing forests to wind damage. Among these, tree height has been consistently identified as the primary factor, while tree species, soil properties, and landscape characteristics also play significant roles (Gardiner, 2021; Gardiner et al., 2010). Knowledge of factors that increase the likelihood of forest wind damage enables forest managers and planners to mitigate wind damage through tree species selection, management, and planning measures.

Various methodologies have been employed to explain wind damage to forests, including analysis of spatially distributed forest growth and yield plots (Albrecht et al., 2012; Valinger and Fridman, 2011), wind tunnel experiments (Gardiner et al., 2005; Poëtte et al., 2017), mechanistic modelling (Blennow and Sallnäs, 2004; Peltola et al., 1999), and statistical and machine learning approaches (Albrecht et al., 2012; Blennow and Olofsson, 2008; Hale et al., 2015; Hanewinkel, 2005; Hanewinkel et al., 2004; Hart et al., 2019; Pawlik and Harrison, 2022).

Statistical modeling and machine learning modeling of wind damage utilize observed wind damage and input variables, including meteorological, topographical, surface, soil, and forest stand variables (Díaz-Yáñez et al., 2019; Hanewinkel et al., 2014; Pawlik and Harrison, 2022; Saarinen et al., 2016; Schindler et al., 2016; Suvanto et al., 2019). These approaches require a large amount of wind damage observations and high-resolution weather models accurately representing the atmospheric situation.

Modelling approaches to forest wind damage have so far focused on wind, i.e. the horizontal component of the airflow, acting on the trees (Chen et al., 2018; Dupont et al., 2015; Hart et al., 2019; Kamimura et al., 2022; Peltola et al., 1999). However, in mountainous terrain, mountain wave events are known to occur when stably stratified air flows over mountains (Durran, 1990), characterized not only by strong wind, but also by air being forced to rise and cool as it follows constant lines of potential temperature which is affected by the orography, typically lifted upward on the windward side and downward on the leeward slopes (Lilly and Klemp, 1979; Queney et al., 1960). This airflow pattern can lead to the formation of atmospheric gravity waves, characterized by alternating bands of rising and sinking air, both above and, in some situations, on the lee side of the mountains. These waves are often associated with intense and turbulent air movement on the leeward side, with speeds that can reach 60 m s^{-1}, two to three times higher than the summit wind speed. Known as downslope windstorms (Jackson et al., 2013), these phenomena can cause severe turbulence, downdrafts, and abrupt changes in airflow direction and speed on the lee side of the mountains, resulting in damage to forests and infrastructure.

Reports exist of local mountain wave events in western North America causing substantial forest damage (Meyers et al., 2003). Similar weather phenomena have been routinely observed in Norway, though not specifically linked to forest damage – in part, because the affected areas lacked any significant productive forest cover (Harstveit et al., 1995; Sandvik and Harstveit, 2005). Increased resolution of numerical weather prediction (NWP) models in recent years has enabled the realistic simulation of weather phenomena influenced by orography, such as mountain waves (Samuelsen and Kvist, 2024) and channeled flows in valleys (Valkonen et al., 2020). To the best of our knowledge, no previous studies have attempted to explain forest damage caused by a mountain wave event, through either mechanistic modelling, statistical techniques, or machine learning approaches.

Because orographic features impose systematic spatial patterns on the airflow, wind disturbance processes in neighboring forest stands are often correlated. This introduces the broader problem of spatial autocorrelation, a well-known issue in geostatistics (Moran, 1950). Spatial autocorrelation arises when predictor variables vary systematically in space, reducing the independence of observations and potentially biasing model performance. For example, when specific combinations of predictor variables are overrepresented due to dense sampling at small spatial intervals, this can inflate both predictive accuracy and explanatory power of statistical or machine learning models. Despite its potential importance, no systematic efforts have, to the best of our knowledge, been made to account for spatial autocorrelation in empirical wind damage studies aimed at identifying factors that predispose forests to disturbance. Therefore, models that explicitly account for spatial autocorrelation could provide more accurate insights into the factors contributing to forest wind damage.

In this study, we tested two hypotheses as follows:

1. Forest stand properties do not significantly contribute to explaining forest damage during a mountain wave event.
2. Meteorological variables related to atmospheric stratification, turbulence, and non-horizontal airflow significantly contribute to explaining forest damage during a mountain wave event.

Our analysis assumes that high resolution NWP models can give a realistic representation of the airflow during mountain wave events (Samuelsen and Kvist, 2024; Valkonen et al., 2020). We proceed from the premise that in mechanistic forest wind damage models, the main drivers of variance in the critical wind speed (CWS) exceeding which causes a tree to overturn or breakage are tree height and stem diameter (Locatelli et al., 2017). We further assume that when a forest stand is exposed to non-horizontal airflow, a dense canopy, with a larger surface to intercept the airflow, makes the stand more susceptible to wind damage (Quine et al., 2021). Using data from the 19 November 2021 windstorm in southeastern Norway, we utilize input data comprising field observations of wind damage and forest inventories based on airborne Light Detection And Ranging (LiDAR) surveys. Our analysis employs the Random Forest modeling method (Breiman, 2001), interpreting variable importance using the SHapley Additive exPlanations (SHAP) approach (Lundberg and Lee, 2017; Lundberg et al., 2018; Shapley, 1953), while accounting for spatial autocorrelation (Anselin, 1995) in model formulation and accuracy assessment.

2. Materials and methods

2.1. Mountain wave event, study area, and forest damage observations

On 19 November 2021, a deep low-pressure system brought westerly flow with relatively warm air aloft over southern Norway (Fig. 1(a) and (b)), creating favorable conditions for the formation of mountain waves and potentially downslope windstorms on the lee side of the Scandinavian Mountains. Weather stations at Geilo (772 m a.s.l.), Nesbyen (166 m a.s.l.), and Veggli (275 m a.s.l.), all located in valleys at a range of elevations (Fig. 1(a)), recorded increasing wind from early morning with maximum gusts of 32.0 m s^{-1}, 25.3 m s^{-1}, and 24.9 m s^{-1} respectively during the afternoon (Skattør et al., 2021). Although the weather situation was well predicted on a synoptic scale and weather alerts were issued, some areas experienced stronger winds than forecasted.

The strong gusts observed in the mountain valleys in southern Norway are likely to have been brought by downslope windstorms

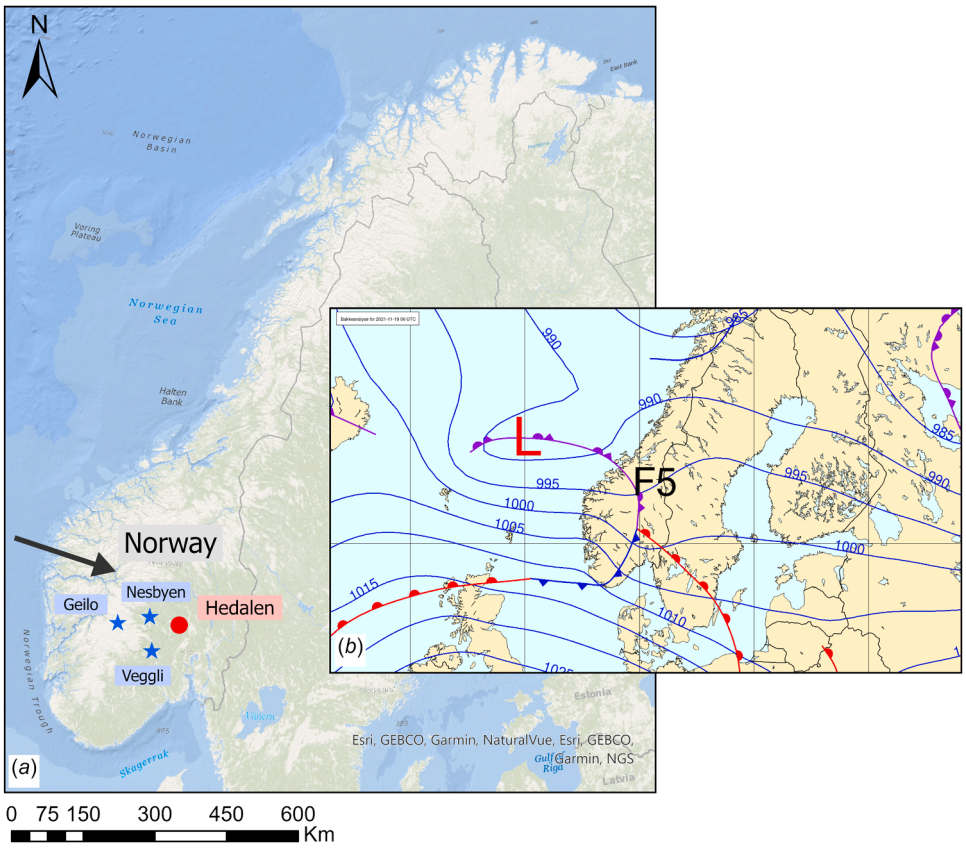

Fig. 1. (a) Location map of the study area (red dot symbol), including locations of the three weather stations at Geilo (WIGOS ID 0–20,000–0–01,359), Nesbyen (WIGOS ID 0–20,000–0–01,373), and Veggli (WIGOS ID 0–20,000–0–01,471) (blue star symbols) and the main wind direction (black arrow); (b) mean sea level pressure (MSLP) analysis valid 19 November 2021 0600 UTC showing the deep low-pressure system approaching eastern Norway. MSLP isobars in hPa are shown in blue. F5 indicates 5 hPa decrease in MSLP in the past 3 h that can be associated with the development or strengthening of a severe weather system.

associated with mountain wave formation and further downward mixing of momentum to the ground surface. Mass et al. (2019) report that strong wind shear and a low temperature inversion base, close to the height of the upstream terrain, favor localized downslope winds and irregular flow pattern on the lee side. Fig. 2 illustrates the necessary conditions for mountain waves to form, as described in Durran (1990)—

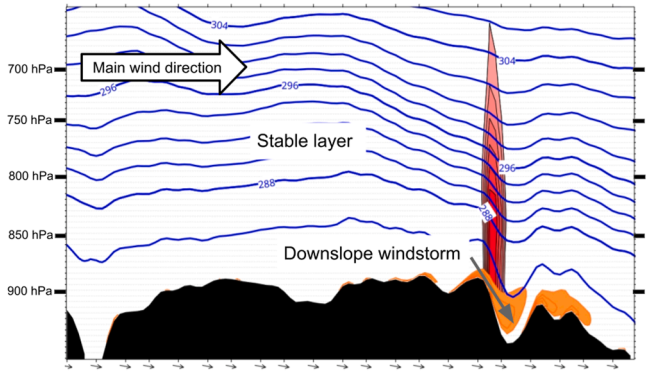

Fig. 2. Conceptual diagram of flow over mountain leading to the formation of mountain waves and downslope windstorms. The stable layer aloft, indicated by tightly spaced isentropes (in blue) starting at approximately 850 hPa with a strong vertical increase in potential temperature, is necessary for the waves to form, while the mountain wave manifests itself in the sinking air over the lee side of the mountain (high absolute values of upward air velocity indicated by red shading), giving rise to a downslope windstorm characterized by high TKE values. Orange shading shows areas where the square root of TKE exceeds 5 m s^{-1}.

the main wind direction is across the mountain range and there is a stable layer aloft giving buoyant oscillations and hence air descending over the valley on the lee side, where the downslope windstorm manifests itself as gusty wind extending down to the valley bottom, as indicated by the high values of turbulent kinetic energy (TKE) on the leeward side of the mountains in Fig. 2.

Wind damage from the 19 November 2021 windstorm was widespread in south-eastern Norway (Skattør et al., 2021), affecting buildings, utility and telecommunications infrastructure, as well as forests. There were reports of broken Scots pine trees aged over 100 years (Viken Skog, 2021). Forest damage was highly localized, with multiple clusters of severe impact. The total extent of forest damage was estimated at 2.4 to 2.6 million m^3, primarily due to uprooting (Skogbrand Forsikringsselskap Gjensidig, 2022b). Among the hardest-hit areas was the Hedalen valley in Sør-Aurdal municipality (Fig. 1(a)). Covering 105 km^2, the valley lies in the boreal forest zone at elevations ranging from 290 to 1130 m a.s.l. The valley is characterized by a steep east-facing slope (up to 66° steep) in the west and undulating hilly terrain in the east, with west-facing slopes approximately 25° steep and steeper south-facing ones (up to 45°). The forests are dominated by Norway spruce (*Picea abies* (L.) H. Karst, 74 %) with an admixture of birch (*Betula pubescens* Ehrh. and *B. pendula* Roth., 8 %) in the valley bottom and sides at elevations below 450–500 m a.s.l., with Norway spruce gradually overtaken by Scots pine (*Pinus sylvestris* L., 19 %) at higher elevations.

Hedalen is a glacial U-shaped valley with the bottom covered by thick (1 m to >10 m) poorly sorted moraine sediment with some fluvial sediment bodies and eskers in the northern and southern ends; peat and bog are also present in the northern half of the valley bottom. At higher elevations, thin moraine sediment interspersed with bedrock outcrops and patches of peat and bog are typical. In terms of land-use types,

agriculture, forestry, and rural settlements prevail in the northern half of the valley, while the southern half is dominated by forestry land use. At elevations above 500 m a.s.l., production spruce-pine forest transitions into sparse high-elevation pine forest wilderness.

We used a ground reference dataset containing observations of windthrow damage collected during the winter of 2021/2022. The ground reference was a combination of visual interpretation of drone orthomosaics and field observations. Windthrow damage was mapped as vector polygons by the Norwegian forestry insurance company Skogbrand with the goal to identify areas eligible for insurance compensation where the eligibility criteria were overturning and breakage due to strong wind in at least 25 % of the pre-storm tree count, excluding patches smaller than 0.2 ha and stands with fewer than 200 stems ha^{-1} (Skogbrand Forsikringsselskap Gjensidig, 2022a). One third of the damage polygons were reported as partially damaged, i.e., with less than 50 % of the pre-storm tree count felled by wind. Because of the observed inconsistencies in the application of the damage level criterion in the field data, we chose to merge the two damage classes (i.e., total and partial damage) together.

No-damage areas were identified by combining the areas representing forest estates covered by a wind damage insurance, a forest mask derived from the Norwegian forest resource map SR16 (NIBIO, 2024), and the damage polygons, assuming forest areas covered by insurance and not reported as damaged to be free of windthrow damage. The resulting damage and no-damage polygons were rasterized on a 16 × 16 m grid aligned with the SR16 map grid for a total of 40,000 damage and 42,000 no-damage cells. The number of no-damage cells was selected to achieve a prevalence of close to 0.5 for the entire dataset. The reference dataset covered 29 % of the forest area. The reference data collection, processing, and subsetting procedure is described in more detail in Zubkov et al. (2023).

Fig. 3 presents a map of the windthrow damage areas used in this study together with maximum wind (Fig. 3(a)) and wind gust (Fig. 3(b)) speed values at 10 m altitude during the entire observation period on 19 November 2021. Hourly wind speed in the valley bottom, where most of the wind damage occurred, did not exceed 20 $m\ s^{-1}$; higher estimated wind loads can only be found at elevations above 1000 m a.s.l., i.e. mostly above the tree line, in the west of the study area. Basic statistics of the valley's forests derived from the SR16 forest resource map are presented in Fig. 4 for damage and no-damage class separately.

Finally, we used the Norwegian forest resource map SR16 to extract three forest structure variables (Table 1) as follows aggregated on a 16 × 16 m grid: (1) mean tree diameter at breast height (DBH), estimated for trees with a DBH ≥ 8 cm (*DBH8*), (2) tree crown coverage as a percentage of the SR16 cell area (*CC*), (3) dominant tree height in dm (*OH*). SR16 forest structure estimates are derived from recent airborne LiDAR

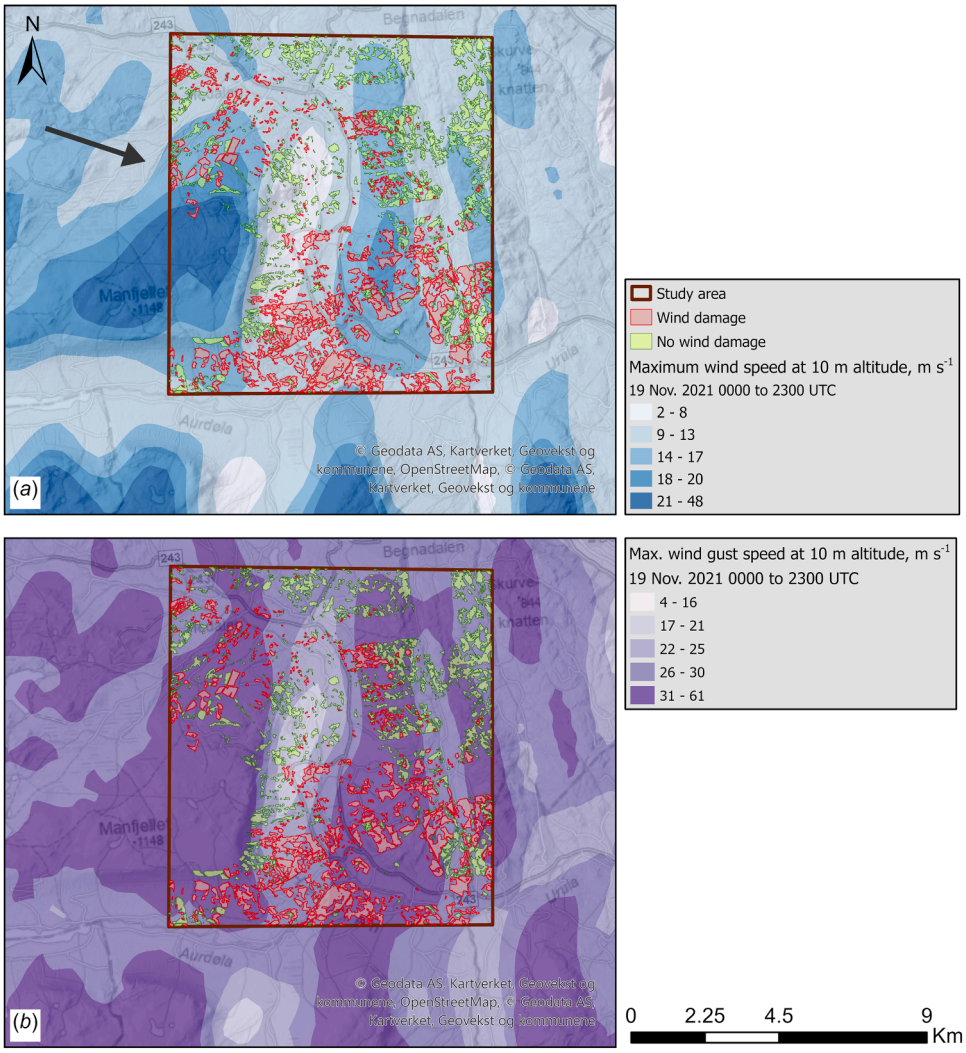

Fig. 3. Map of damage and no-damage areas and hourly (a) wind and (b) wind gust speed at 10 m altitude in the study area aggregated to the maximum value over the observation period of 19 November 2021 0000 to 2300 UTC. Wind and wind gust speed data were extracted from the 500 m HARMONIE-AROME NWP model used in this study. Black arrow shows the main wind direction.

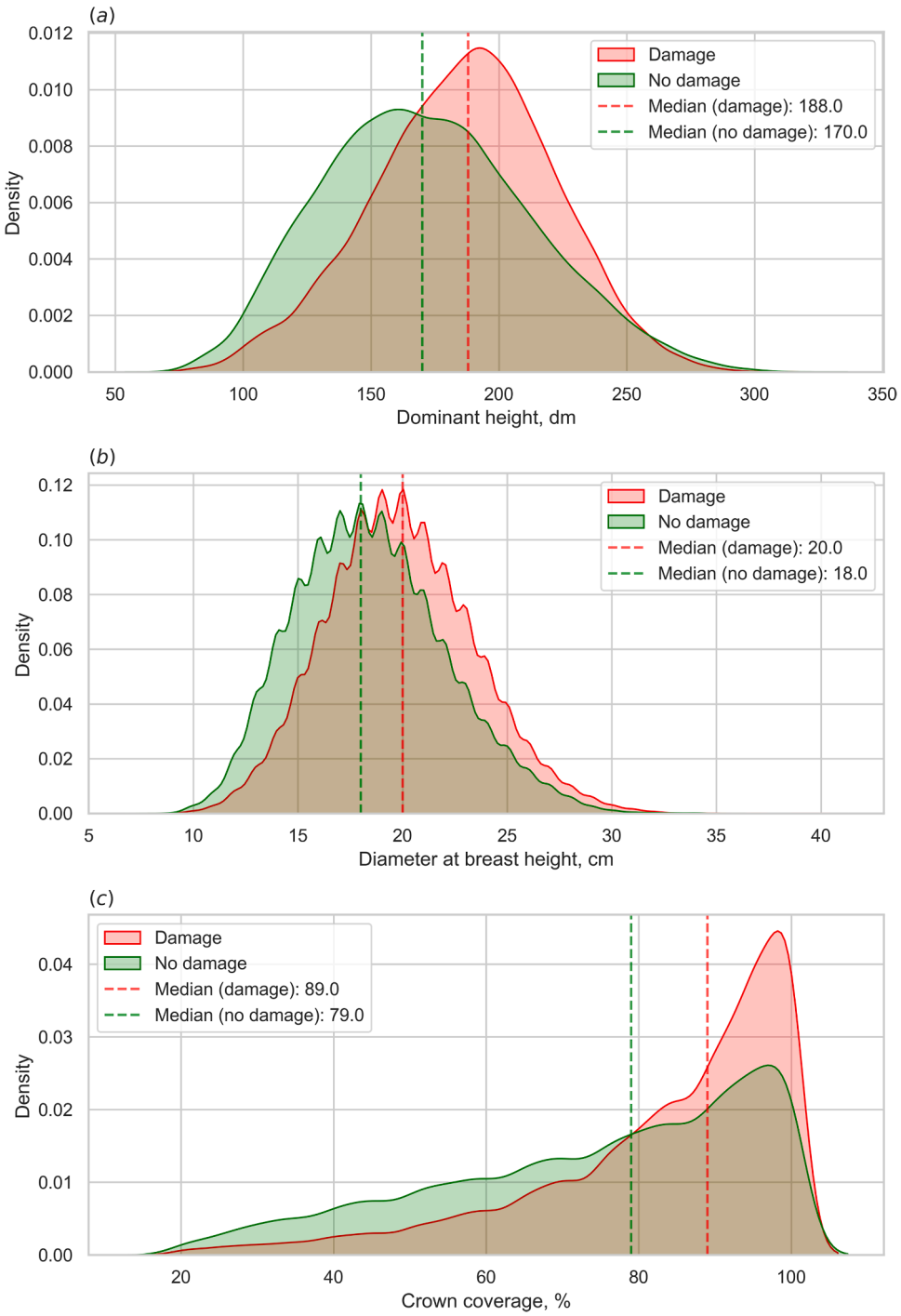

Fig. 4. Density plots of the main forest structure variables in the study area stratified by observed wind damage: (a) dominant height in dm, (b) tree diameter at breast height in cm (for trees with stem diameter $\geq$ 8 cm), and (c) crown coverage percentage.

surveys augmented with multispectral aerial and satellite imagery used for stratification into tree species. While multiple forest structure variables are available from the SR16 map, we chose *OH* and *DBH8* as these were previously reported as the main drivers of variance in predicted CWS (Locatelli et al., 2017), while *OH* and *CC* are both derived from direct measurements of forests using, respectively, LiDAR and multispectral optical remote sensing. *CC* was chosen to represent the sail area of a forest canopy when exposed to non-horizontal airflow.

Considering the spatial distribution of wind damage in the study area (Fig. 3), which could be found in flat and steep terrain at lower and higher elevations alike, we chose not to include topographical variables, such as slope, slope aspect, and elevation, into the dataset. The decision was guided by an observation that the wind damage pattern across eastern Norway after the 19 November 2021 windstorm appeared to be driven by large-scale landscape forms, such as mountain ridges, valleys, and lee-side slopes, rather than local-scale variations in topography in forested areas.

2.2. *High-resolution weather model*

Modern weather forecasting relies to a large degree on the use of NWP models. In an NWP model, a short-term forecast is combined with

Table 1
Forest structure (SR16) variables and aggregated atmospheric variables used as predictive features.

Notation	Unit	Variable description
Forest structure variables aggregated over the SR16 grid		
DBH8	cm	mean tree DBH for DBH $\geq$ 8 cm
CC	%	tree crown coverage as a fraction of a 16 $\times$ 16 m cell area
OH	dm	dominant tree height
Atmospheric variables aggregated over the observation period of 10 to 18 UTC on 19 November 2021		
FG10_max	m s^{-1}	maximum FG_{10}
w_max	m s^{-1}	maximum absolute *w*
θ_diff_ml10_max	K	maximum θ gradient between 30 m and 220 m above the model terrain
θ_diff_ml10_min	K	minimum θ gradient between 30 m and 220 m above the model terrain
θ_diff_850hpa_max	K	maximum θ gradient between the pressure levels 850 and 900 hPa
θ_diff_850hpa_min	K	minimum θ gradient between the pressure levels 850 and 900 hPa
TKEdiff_min	m^2 s^{-2}	minimum difference in TKE between 30 m and 220 m above the model terrain

data from meteorological stations, weather satellites, radiosondes, and other available observations to characterize the present condition of the atmosphere in a process called data assimilation, and from the initial state, a forecast is calculated by numerically solving the equations representing the atmosphere's physical and dynamical processes.

The national weather services in Scandinavia have adopted for operational forecasting purposes the MetCoOp Ensemble Prediction System (MEPS) model, an implementation of an ensemble prediction system (EPS) version of the HARMONIE-AROME model (Bengtsson et al., 2017; Frogner et al., 2019). MEPS has a 2.5 km horizontal grid spacing and 65 vertical layers, extending from 12 m above the surface of the model terrain to a height of 33 km (Müller et al., 2017). The model's lower levels follow the terrain, with a hybrid coordinate system approximating pressure coordinates at higher levels. The dynamical core of HARMONIE-AROME (Bénard et al., 2010) solves the Eulerian equations describing atmospheric motion on a 2.5 km grid, while atmospheric processes such as radiation, cloud microphysics, and turbulence are parametrized and handled by the model physics (Bengtsson et al., 2017). The handling of turbulence is mainly based on Lenderink and Holtslag (2004) with some modifications as described in Bengtsson et al. (2017). The calculation of TKE is specifically based on a parameterization of shear, buoyancy, transport, and dissipation as explained in Lenderink and Holtslag (2004), while the physical processes in the surface and the interaction between surface and atmosphere is treated by SURFEX (Masson et al., 2013), which is a surface model including land cover from ECOCLIMAP (Rieutord et al., 2024).

Following Valkonen et al. (2020), who demonstrated that increasing model resolution from a 2.5 km to 500 m grid spacing in Adventdalen, Svalbard, significantly reduced modeled wind error and produced a more realistic wind pattern, we were motivated to rerun HARMONIE-AROME for 19 November 2021 with a 10 s time step at a 500 m cubic grid spacing with 90 vertical layers, starting at 5 m above the surface of the model terrain. The rerun suggested that downslope winds occurred on the lee side of the mountains in southeastern Norway.

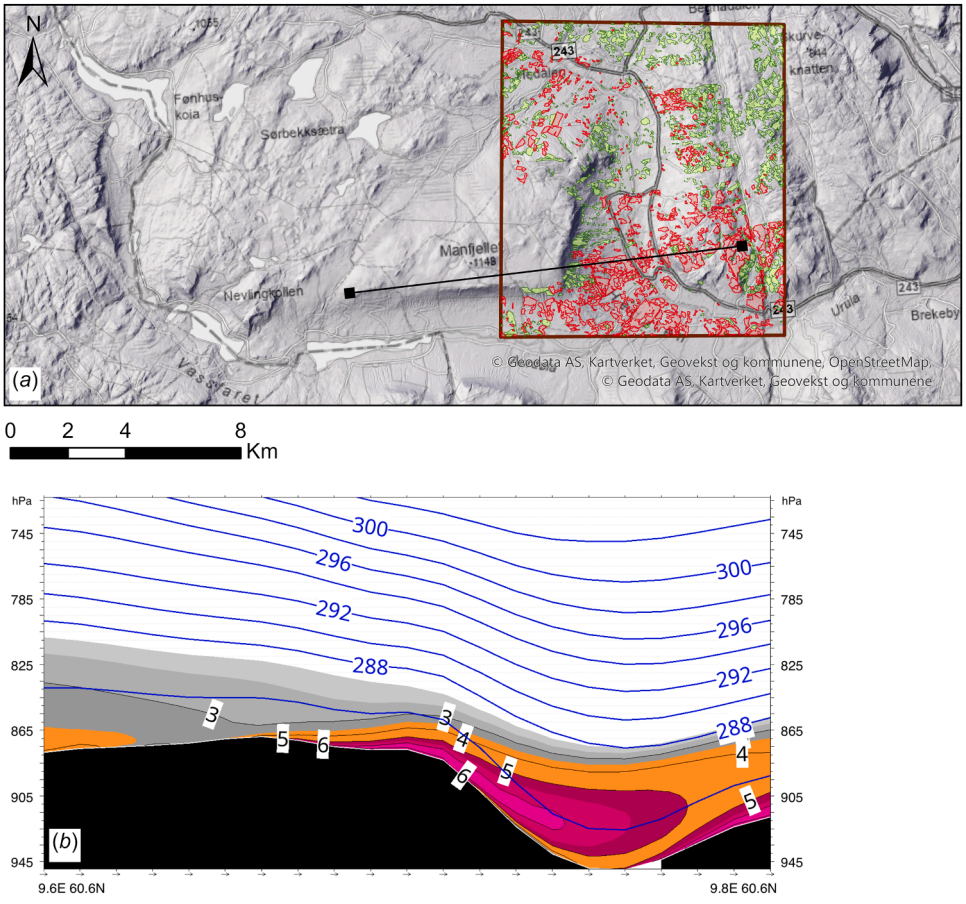

Fig. 5. (a) Hillshade map of the Hedalen valley showing the study area and the location of the cross section in (b). See Fig. 3 for the map legend. (b) Cross section of potential temperature (in blue) in kelvins (K) and square root of turbulent kinetic energy ($\sqrt{TKE}$) in m s^{-1} (values in black; shaded gray $<$ 3.5 m s^{-1}, orange 3.5–5 m s^{-1}, purple $\geq$ 5 m s^{-1}), valid 19 November 2021 1500 UTC when the high TKE pattern on the lee side of the mountain was most expressed. Altitudes 30 m and 220 m referred to in this study are just above the model ground surface (shown in black) and just below the lowest 286 K isentrope.

A cross-section of potential temperature, square root of TKE, and tangential wind velocity across the valley of Hedalen (Fig. 5) reveals relatively high TKE values, indicating strong turbulence on the lee side.

The model outputs hourly variables, and a selection of these were aggregated over the time interval of 10 to 18 UTC on 19 November 2021 to maximum and/or minimum values per grid cell (Table 1):

(1) hourly wind gust speed at 10 m altitude (FG10) in m s-1, which is the conventional observation height for wind and gust at meteorological stations. In the HARMONIE-AROME model, gust is calculated as follows (Kurbatova et al., 2018):

$$FG_{10} = FF_{10} + a\sqrt{TKE_{20}}, \quad (1)$$

where FF_{10} is 10-minute average wind speed at 10 m altitude in m s^{-1}, TKE_{20} is turbulent kinetic energy at 20 m altitude in m^2 s^{-2}, while a is a constant of 3.5 which was statistically adjusted to fit the observations of wind gust speeds in Norway. TKE is, in turn, defined as:

$$TKE = \frac{1}{2}\left(\sigma_u^2 + \sigma_v^2 + \sigma_w^2\right), \quad (2)$$

where σ_u^2, σ_v^2, and σ_w^2 represent the variances of the latitudinal (u), longitudinal (v), and vertical (w) airflow velocities in m s^{-1}.

(2) Upward air velocity in m s^{-1} representing w at an altitude of 220 m above the surface of the model terrain. We used w in combination with potential temperature (θ), FF_{10}, FG_{10}, and TKE to identify areas where mountain waves were present. The absolute value of w was used for analysis, representing both the downward airflow and the upward flow generated by mountain waves (Jackson et al., 2013).
(3) Potential temperature gradients in K close to the ground and higher in the atmosphere, namely approx. 30 m and 220 m above the model terrain, *θ_diff_ml10* and *θ_diff_ml10*) and between the pressure levels 850 and 900 hPa (*θ_diff_850hpa* and *θ_diff_850hpa*). A steep vertical gradient in potential temperature is an indicator of potential temperature isosurfaces (isentropes) pressed together and stable layering in the atmosphere, which can be conductive to gravity wave formation (Jackson et al., 2013). Mountain waves would be expected to form in areas with a steep vertical potential temperature gradient aloft, while when close to the ground, a steep gradient can prevent the strong wind from reaching the ground surface.
(4) Difference in TKE in m^2 s^{-2} (*TKEdiff*) at 30 m and 220 m above the model terrain. Under neutral stratification, TKE is expected to exhibit a negative vertical gradient, meaning higher values near the ground compared to higher altitudes. This pattern is primarily attributable to surface roughness or friction. In contrast, a positive vertical gradient in TKE, identified by strongly negative values of *TKEdiff*, indicates abnormally high turbulence aloft, as shown in Fig. 5(b). The specific altitudes 30 m and 220 m were selected based on the orography of the study area and the vertical stratification of the atmosphere, as shown in Fig. 5, where the former captures TKE near the ground surface, while the latter contains the high TKE zone on the lee side of the mountain and in the downstream area across the valley.

2.3. Data sampling and model training

The spatial distribution of forest damage observations showed a clear predominance of no-damage cells in the north-eastern part of the study area. This part of the study area is characterized by hilly terrain at elevations up to 800 m a.s.l., sparse forest cover, and little variation in the atmospheric variables selected for further analysis. The central and south-western parts of the study area had a heterogeneous mix of damage and no-damage cells, with locally dominant damage observations and a greater variation in elevations, forest structure, and atmospheric conditions. To address the spatial patterns and varying levels of spatial autocorrelation, we applied two different minimum sampling intervals: 500 m for the north-eastern part (sparse coverage) and 200 m for the rest of the area (dense coverage). Spatially constrained sampling and geostatistical analysis were performed in ArcGIS Pro 3.2 (ESRI, 2024).

The pseudo-random sampling procedure using a random number stream from a random number generator and seed was repeated 20 times for the purpose of subsequent cross-validation of the models, resulting in 512 data points in each fold, with approximately equal representation of the damage and no-damage classes, for a total of 10,000 data points. For each resulting fold, we split the data into training and test subsets using an 80/20 ratio and trained a Random Forest classifier with the default hyperparameters as implemented in the scikit-learn package for Python (Pedregosa et al., 2011), followed by hyperparameter optimization using randomized search. For model performance assessment, we recorded the out-of-bag (OOB) area under the receiver operating characteristic curve (ROC AUC) for the training subset and the ROC AUC for the test subset in each fold. We then averaged these values over the 20 folds. ROC AUC is a metric commonly used to measure a model's ability to discriminate between binary classes and does not require a pre-defined threshold value to separate the classes. The metric can have values between 0.5 (discrimination ability no better than by random chance) and 1 (perfect discrimination, equivalent to a true positive rate of 1 and a false positive rate of 0).

To minimize the effect of information leakage on our assessment of the individual input variables' impact on model performance, we used hierarchical clustering based on how interchangeable the variables are in explaining the outcome, as implemented in the Python SHAP package (Lundberg and Lee, 2017). We iteratively applied a clustering cut-off threshold of $d_{\min} = 0.5$ with single linkage and the SHAP values of the model variables in each successive iteration to reduce the number of features from the initial set listed in Section 2.2. SHAP values (ϕ), derived from Shapley values in cooperative game theory and introduced in Lundberg and Lee (2017), help in interpreting a machine learning model's predictions by quantifying the effect of each feature on the overall prediction. Shapley values (Shapley, 1953) account for how each feature affects the prediction by averaging its impact across all possible combinations with other features. If a feature, based on its mean ϕ and $d_{\min}$, was identified as a candidate for being excluded from the feature set, a permutation test with 1000 permutations (smallest resolvable pseudo p value $1/(1000 + 1) \approx 0.001$, corresponding to >99.9 % confidence) was carried out. The mean pseudo p value for the test ROC AUC values was then calculated across the folds. We repeated this procedure iteratively, removing one feature at a time, until no features were left having both low mean ϕ and $d_{\min}$ relative to other features and pseudo $p > 0.05$ (i.e. applying a 95 % confidence threshold).

2.4. Spatial autocorrelation analysis and model interpretation

One of the optimized models was randomly selected for interpretation to explain the observed forest damage and the main predisposing factors. First, we calculated the model's residuals, defined as the difference between the observed binary class value and the estimated probability of damage. Model residuals were examined for spatial autocorrelation by calculating the Anselin Local Moran's I using the Cluster and Outlier Analysis tool in ArcGIS Pro 3.2. The method identifies statistically significant clusters of high ("hot") and low ("cold") values as well as outliers, i.e. highs surrounded by lows and vice versa (Anselin, 1995). The Anselin Local Moran's I statistic is a localized version of the global Moran's I requiring that a neighborhood be defined using methods such as a fixed distance, number of neighbors, or spatial weights. In this study, we chose to define neighborhoods using a threshold distance of 1 km with inverse distance squared weighting. We then applied a false discovery rate (FDR) correction and performed 999

permutations (confidence level >99.9 %) to calculate a pseudo p value for each of the identified clusters and outliers.

Second, for the interpretable machine learning approach, we used the SHAP values calculated for the final model's features to explain the effect of individual features on the model's prediction for each observation. SHAP values describe both the direction (positive or negative) and magnitude of the feature's effect, and are additive, i.e. they add up to the difference between the predicted outcome and the baseline prediction without any of the model's features.

3. Results

To test our hypotheses regarding the relationships between atmospheric and forest variables and observed wind damage, we employed a Random Forest classification model. The model outputs were interpreted using SHAP values to identify the most influential predictors, and the resulting spatial patterns of predicted and observed damage were further examined using Anselin Local Moran's I analysis.

3.1. Model features and feature importance

We first trained a baseline Random Forest model using the entire set of 10 input features to predict forest storm damage. The model exhibited a reasonable ability to discriminate between the damage and no-damage classes with a mean ROC AUC across the 20 folds of 0.86 (SD = 0.02) on the OOB train subset and 0.83 (SD = 0.03) on the test subset. Minimum potential temperature gradient aloft (*θ_diff_850hpa_min)* had the highest SHAP value of 0.13, indicating the strongest impact on the model's predictions. In contrast, all forest features had a mean SHAP value below 0.03 and strong hierarchical clustering was found between *DBH8* and *OH* (Fig. 6), with $d_{min} < 0.4$, suggesting limited contribution to the model and high redundancy.

In an iterative model refinement process, we successively excluded the forest structure features *CC* (pseudo $p = 0.44$) and *OH* (pseudo $p = 0.28$) and the meteorological features *θ_diff_ml10_min* (pseudo $p = 0.18$), *TKEdiff_min* (pseudo $p = 0.22$), *θ_diff_ml10_max* (pseudo $p = 0.16$), and *θ_diff_850hpa_max* (pseudo $p = 0.22$), guided by their low d_{min} and ϕ_{mean} and statistically insignificant permutation pseudo p values. The resulting four-feature model combining meteorological variables with *DBH8* achieved a mean ROC AUC of 0.81 (SD = 0.02) and 0.82 (SD = 0.04) on the OOB and test subsets, respectively. The potential temperature gradient *θ_diff_850hpa_min* remained the single most important feature, with its ϕ_{mean} value of 0.19 close to that of the other features combined.

After excluding *DBH8* (pseudo $p = 0.15$), the final three-feature model trained on meteorological features alone achieved a ROC AUC of 0.80 (SD = 0.03) and 0.81 (SD = 0.04) on the OOB and test subsets, respectively (Table 2). The decrease in the model's ROC AUC on the test subset was not found to be statistically significant (pseudo $p = 0.15$, Table 2). After hyperparameter optimization, the resulting model showed mean performance comparable to that of the baseline ten-feature model.

False negative predictions in the three-feature model were mostly found in the transition zones between areas dominated by either damage or no-damage observations, while false positives were present either scattered among dominant true positives in the southern part of the area or in the north-eastern corner where few observations of wind damage

Table 2
Mean SHAP values (ϕ_{mean}), hierarchical clustering distances (d_{min}), mean pseudo p values of permutation tests (1000 permutations) of the meteorological features in the three-feature model and the resulting mean ROC AUC across 20 folds, incl. mean ROC AUC after hyperparameter optimization and cross-validated mean ROC AUC.

Feature	ϕ_{mean}	d_{min}	Mean pseudo p (SD)
θ_diff_850hpa_min	0.20	0.87	< 0.001 (< 0.001)
FG10_max	0.08	0.87	0.03 (0.05)
w_max	0.07	0.87	0.05 (0.06)
Mean ROC AUC OOB/test (SD)	0.8 (0.03) / 0.81 (0.04)		
Mean ROC AUC (SD) on the test subset after hyperparameter optimization / Mean cross validated ROC AUC, $k = 20$	0.83 (0.03) / 0.84		

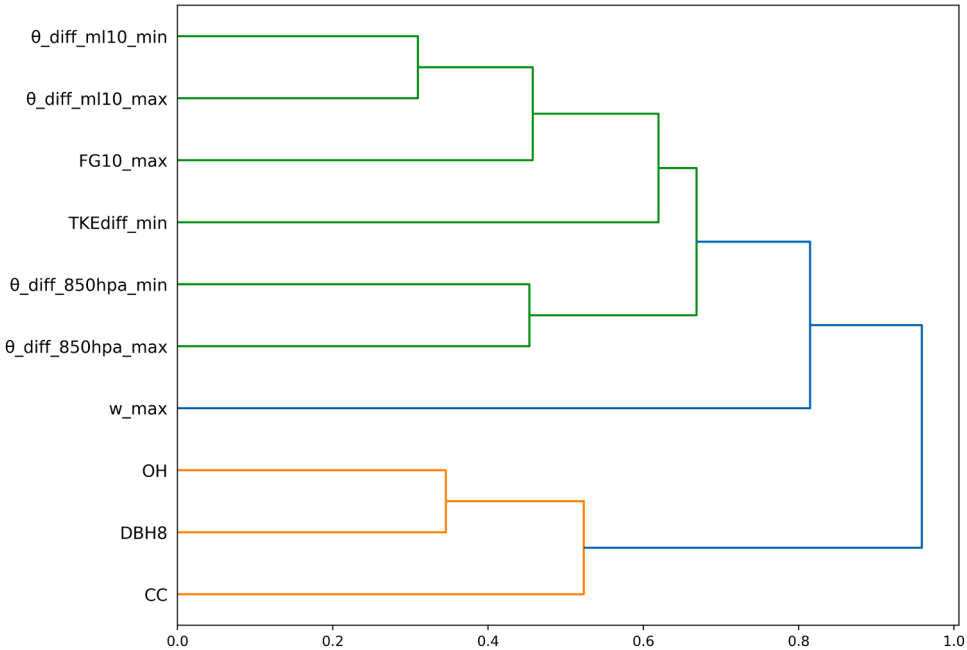

Fig. 6. Hierarchical feature clustering dendrogram of the baseline Random Forest model trained on the full set of ten meteorological and forest structure features. Branch colors in the dendrogram denote clusters formed by the model features in predictive similarity space, with distances (on the x-axis) defined as $d = 1 - R^2$, where R^2 quantifies the similarity of feature-specific XGBoost models in explaining the outcome (Lundberg and Lee, 2017).

exist (Fig. 7).

3.2. Spatial autocorrelation

Anselin Local Moran's I analysis of the model residuals revealed a minor residual autocorrelation in the model residuals, specifically in the low-low (LL) clusters, i.e. datapoints with a low residual error showing a statistically significant (pseudo $p < 0.001$) spatial clustering pattern. We found two such LL clusters—one in the south-central part of the area, coincident with a large continuous area of wind damage, and another one on the steep mountainside in the west-central part of the area (Fig. 8). Smaller high-high (HH) clusters were mainly observed in those areas where wind damage observations are interspersed with no-damage observations, such as in the north-west and south-east of the study area. Across all folds, the majority of the residuals had no statistically significant spatial pattern, with LL clustering being the most common pattern, where observed (Table 3).

3.3. Model interpretation

The potential temperature gradient (*θ_diff_850hpa_min*) had the strongest impact on the model predictions, with high minimum values of the gradient increasing the probability of wind damage (Fig. 9(a)). High absolute vertical air velocity (*w_max)* was associated with strongly negative SHAP values, suggesting it reduces storm damage probability, contrary to the intuitive expectation that strong non-horizontal airflow causes severe forest damage. The impact of wind gust (*FG10_max*) was more in line with an intuitive understanding, with high feature values increasing the probability of wind damage. The decision plot in Fig. 9(b) demonstrates that it is mainly *θ_diff_850hpa_min* and *FG10_max* that control the discrimination between the damage and no-damage class.

The two features contributing strongly to false negatives by shifting probabilities towards lower values are *θ_diff_850hpa_min* and *FG10_max*, while false positive predictions are mostly driven by *θ_diff_850hpa_min* and *w_max,* shifting the model output towards higher damage probability. Considering its high mean SHAP values, *θ_diff_850hpa_min* had the strongest contribution to the model's misclassifications.

3.4. Hypothesis testing

We tested H.1, stating that forest stand properties do not significantly contribute to explaining forest damage during a mountain wave event, by incorporating the forest stand variables diameter at breast height (*DBH8*), dominant tree height (*OH*) and crown coverage (*CC*) as features in the Random Forest model. The inclusion of these forest stand variables did not bring a significant improvement in the model's predictive performance (pseudo $p = 0.15$ for *DBH8* as the last to be excluded from the four-feature model).

We further tested H.2, stating that meteorological variables related to stratification, turbulence, and non-horizontal airflow significantly contribute to explaining forest damage during a mountain wave event, as features in the Random Forest model. The variables minimum potential temperature gradient (*θ_diff_850hpa_min*) emerged as the most significant model feature explaining the observed damage patterns (pseudo $p < 0.001$, Table 2), followed by wind gust speed (*FG10_max*; pseudo $p = 0.03$), incorporating the TKE_{20} term (Eq. (1)) characterizing turbulent flow (Eq. (2)), and maximum absolute vertical air velocity (*w_max*; pseudo $p = 0.05$). SHAP analysis further indicated that these meteorological variables had high explanatory power, with a particularly strong contribution from *θ_diff_850hpa_min* (Table 2 and Fig. 9).

4. Discussion

4.1. Wind damage predictions and key model features

In this study, we aimed to examine the widely accepted premise that forest wind damage is primarily explained by horizontal wind speed and its interactions with the forest stand properties (Gardiner et al., 2000;

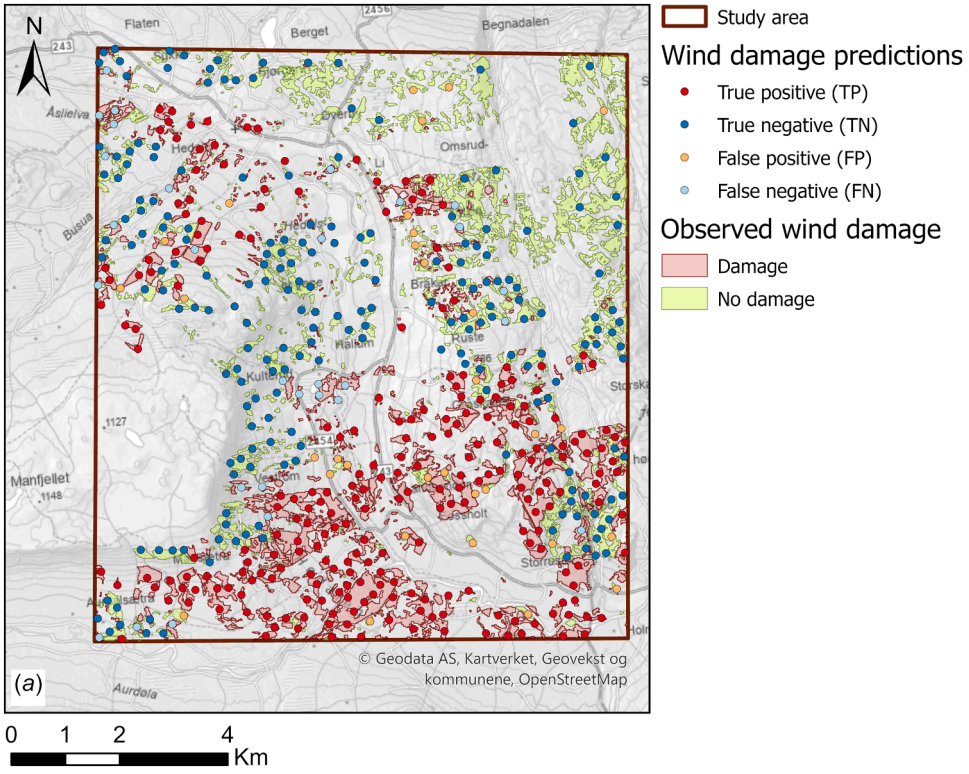

Fig. 7. (a) Wind damage predictions when the three-feature model is applied to the fold $k = 0$ with a probability threshold of 0.5, and (b) the corresponding confusion matrix showing area percentages.

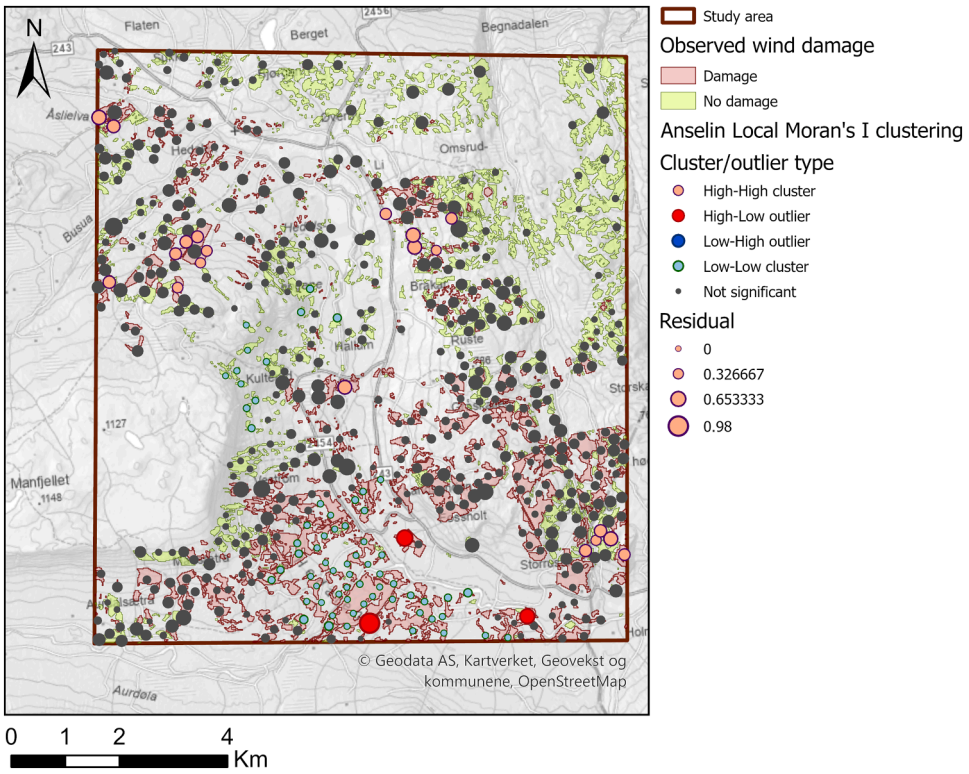

Fig. 8. Anselin Local Moran's I analysis of the three-feature model residuals for a single fold $k = 0$ showing clusters and outliers. Datapoints are sized by the magnitude of the model residuals.

Table 3
Anselin Local Moran's I analysis results across 20 folds on the three-feature model residuals.

	Cluster/outlier pattern						
	High-high clusters	High-low outliers	Low-high outliers	Low-low clusters	Not significant (confidence level 99.9 %)	No neighbors	Total
Count	482	76	132	1561	7866	9	10,126
Percentage	4.76	0.75	1.3	15.42	77.68	0.09	100

Hart et al., 2019; Peltola et al., 1999). Using a case study of a windstorm in southeastern Norway, we tested two hypotheses related to the applicability of this premise in complex mountainous terrain: (1) that forest stand properties do not significantly contribute to explaining forest damage during a mountain wave event, and (2) that meteorological variables related to atmospheric stratification, turbulence, and non-horizontal airflow, significantly contribute to explaining forest damage during a mountain wave event. Our results corroborate both H.1, as evidenced by the lack of a significant improvement in the predictive performance of the model setup that included forest stand properties (pseudo $p = 0.15$ for *DBH8*), and H.2, as indicated by the high significance (pseudo $p \leq 0.05$) and high mean SHAP values of *θ_diff_850hpa_min, FG10_max*, and *w_max* (Table 2).

The approach taken in current mechanistic forest wind damage models, such as ForestGALES (Hart et al., 2019), consists in, first, estimating CWS for a single tree or forest stand and, second, comparing it to a recorded wind speed or a wind speed distribution. Our findings indicate that under certain conditions involving strong vertical airflow due to downward mixing of momentum, such as mountain wave events, horizontal wind speed alone may be insufficient (Fig. 3 and Fig. 4) to explain the wind damage observed on the ground because vertical airflow may significantly increase the magnitude of the total wind vector. Until conventional mechanistic wind damage models have been further developed to take into account three-dimensional forces applied to trees when exposed to turbulent non-horizontal airflow, this study advises caution when applying such models under the described mountain wave conditions as underestimation of forest damage is possible. While horizontal wind speed and forest stand properties remain part of the equation, our results indicate that the most significant explanatory factors for wind damage in mountainous terrain during a mountain wave event are meteorological variables describing atmospheric stratification, turbulence, and non-horizontal airflow. This finds support in Fig. 4 suggesting that the differences in *OH* and *DBH8* distributions between damaged and undamaged forest can explain some, but far from all observed damage. Instead, the minimum potential temperature gradient between the 850 and 900 hPa pressure levels (*θ_diff_850hpa_min*) had the greatest impact on the model's ability to predict forest damage and can be seen as the most direct expression of the downward mixing of momentum exposing the trees to severe wind loads.

Further, the need for a reference wind speed value or distribution that predicted CWS can be compared to can make conventional mechanistic wind damage models difficult to apply under conditions where wind speed may have been underestimated by an NWP model. Inconsistencies between modeled wind speed and observed wind damage in Fig. 3, on the one hand, and forest structure properties in Fig. 4 are an indication that the 19 November 2021 windstorm may be an illustration of such situation. Applying data-driven, machine learning methods like the one proposed in this study may reduce the dependency on accurate horizontal wind speed data.

In our study, horizontal wind speed does play a role in estimating the probability of wind damage under mountain wave conditions, but its

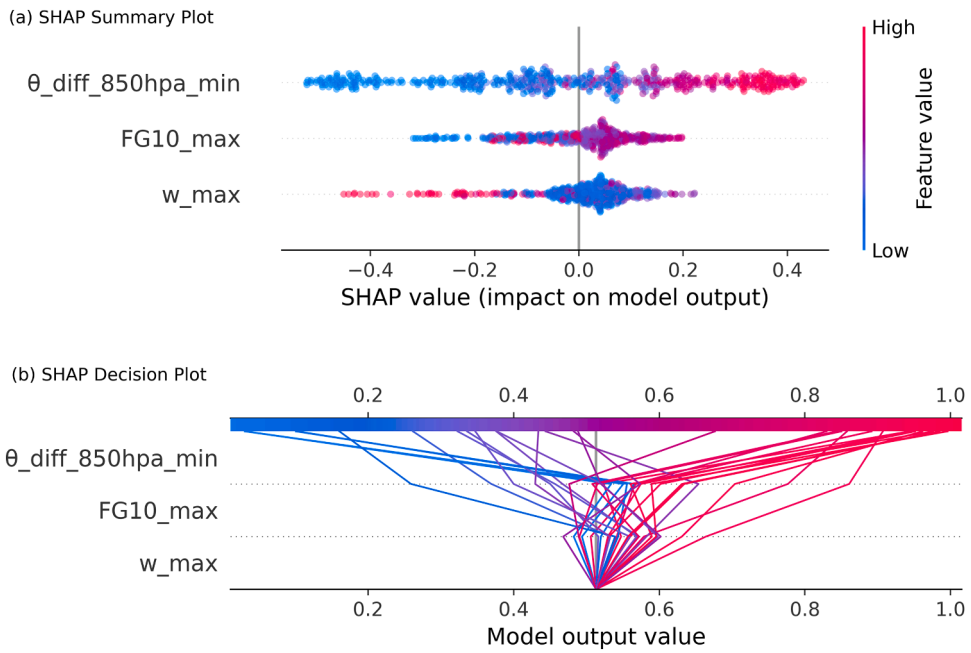

Fig. 9. (a) Bee swarm plot of the SHAP values showing the direction and magnitude of the features' impact on the model predictions in relationship to the feature values, (b) SHAP decision plot for a sample of 50 datapoints, with the bottom x-axis showing the expected probability and the top x-axis indicating the actual predicted probability value; line color denotes the datapoint's predicted outcome.

influence is indirect, primarily contributing as a component of wind gust speed amplified by the TKE term (Eq. (1)). While hourly wind speed alone does not fully account for the observed wind damage pattern (Fig. 3(a)), especially in the severely damaged southern part of the valley bottom, wind gust speed (Fig. 3(b)) has a better correlation with the wind damage map, suggesting that the windthrow damage observed on the ground may have been driven by gusty, turbulent airflow on the mountain's lee side.

Despite this, wind gust speed showed low explanatory power, with SHAP values two to three times lower than that of the potential temperature gradient (*θ_diff_850hpa*) (Table 2 and Fig. 9), and was found to be a strong driver of false negative predictions. The low explanatory power of wind gust speed could explain the exclusion of the TKE gradient in the process of model refinement (see Section 3.1). Notably, during the iterative feature selection process, we aggregated the individual datapoints into mean SHAP values, rather than directly examining their distributions, which may have provided further insights into the effect of extreme SHAP values.

The effect of the upstream terrain on the downstream turbulence is clearly illustrated by Fig. 5 and raises the question of whether the selected model features representing potential temperature and TKE gradients would capture the stable layer and mountain-wave amplification in a different orographic setting. The role of complex upstream orography is also stressed in the existing research on known mountain wave events in Norway, such as Harstveit et al. (1995) and Sandvik and Harstveit (2005), suggesting that the most severe wind damage in Norway is believed to be caused by rotor circulations on the lee side of steep mountains (Grønås and Sandvik, 1999).

Though reports exist of wind gust speed in known downslope windstorm events in Norway potentially reaching 40–60 m s^{-1} (Harstveit et al., 1995; Sandvik and Harstveit, 2005), these are indirect, anecdotal evidence not supported by wind speed records. Still, given the possibility of wind gusts that strong, it is unsurprising that excluding the forest variables had no significant effect on the model's discrimination ability. The critical wind speed values for both Norway spruce and Scots pine are generally reported to be below 30 m s^{-1} (Gardiner et al., 2000), even before accounting for the additional loading from the vertical airflow component.

Our finding of the minimum, rather than maximum, potential temperature gradient *θ_diff_850hpa_min* having the greatest impact on the model's estimated probabilities of damage appears counterintuitive as a strong gradient would be indicative of the presence of a stable layer aloft. This result might, however, need to be interpreted in the context of feature value contrast where the minimum aggregate value allowed for a better separability of damage and no-damage cells. In other words, while a stable layer aloft, characterized by mountain waves with strong downslope wind leading to a steep TKE gradient at a height of 850–900 hPa, persisted through most of the observation period on 19 November 2021, a neutral layer underlying the stable layer leading to downward mixing of momentum was indicative of high turbulence and gustiness, as shown in Fig. 2. Prolonged wind loading and repeated exposure to strong wind loading over a short period can lead to tree failure by gradually weakening root structures and reducing their attachment to the soil. The failure of a single tree can create gaps in the forest canopy, triggering cascading effects that increase the susceptibility of neighboring trees (Dupont et al., 2015; Kamimura et al., 2022).

Known reports (Aune and Harstveit, 1992; Grønås and Sandvik, 1999; Harstveit et al., 1995; Sandvik and Harstveit, 2005; Skattør et al., 2021) of mountain wave events in Norway suggest that downslope windstorms are a violent, though relatively infrequent event, especially in Norway's south-east. Given our finding (Section 3.1 and Table 2) of forest variables having little impact on the probability of forest damage under such events, a potential risk mitigation strategy might consist in identifying areas prone due to the upstream orography to strong downslope winds and adjusting forest management regimes, e.g. shortening the rotation length to account for the increased probability of wind damage (Reed, 1984; Zimová et al., 2020).

4.2. Weather model

The present study of the Hedalen downslope windstorm event indicates that NWP models run at a hectometric grid spacing provide a realistic representation of mountain waves in a terrain that is typical for eastern Norway and hence have the potential to improve forecasts of strong and gusty winds in these areas, which is in accordance with previous studies by, e.g., Samuelsen and Kvist (2024) and Wagner et al.

(2017). The spatial distribution of false model predictions in Fig. 7(a) and the clustering pattern of the model residuals in Fig. 8(a) both indicate that using a higher-resolution digital terrain representation in the NWP model may improve the predictive model's performance as false predictions and HH clusters tend to occur in areas with steep slopes or heterogenous fine-scale orography, e.g. along the valley sides.

The low SHAP values of the TKE gradient in the model iterations and the strongly negative impact of high *w_max* values on the final model's predicted probabilities of damage (Fig. 9(a)) may be an additional indirect indicator of the need for a smaller grid spacing in the NWP model which, with the current 500 m grid, lacks the level of detail required to resolve for the local orography effects on turbulent airflow in the valley sides. Indeed, Mass et al. (2019) found that even a grid spacing of 148 m was too coarse to capture the detailed structure of the downslope windstorm and suggested large-eddy simulations (LES) at a grid spacing of 10 to 20 m.

4.3. Further work

In this study, we examined a specific combination of weather situation and orography. An important next step would be to validate the findings of this study in a different area that was also affected by the 19 November 2021 windstorm in order to assess whether the model formulation and our findings are generalizable to orographic settings other than in the valley of Hedalen and the described stratification conditions in the lower atmosphere conductive to the development of downslope windstorms in forested terrain. Specifically, we expect the choice of pressure levels and altitudes above model terrain used in deriving the potential temperature gradients to be influenced by the local and upstream orography which are known to have a major role in the formation of gravity waves (Jackson et al., 2013).

Validating our findings using a higher-resolution NWP model is another important direction of further research. While 500 m grids offer a considerable improvement when predicting wind and snow damage (Zubkov et al., 2024) compared to operational NWP models using coarser grids, this level of resolution may still be insufficient to capture vertical airflow driven by steep local orography features.

A potential direction for further study is to examine whether the insights into in the role of vertical airflow and atmospheric stratification in predicting and explaining forest wind damage may also be applicable to complex terrain in the absence of mountain waves, when orography effects, such as wind funneling, warrant using high-resolution numerical simulation methods to obtain reliable estimates of airflow in three-dimensional space (Armi and Mayr, 2007). Further, one might want to consider implementing support for modeling applied force in three-dimensional space, including both wind vector magnitude and direction, in the existing mechanistic forest wind damage models, such as ForestGALES (Hart et al., 2019; Quine et al., 2021), HWIND (Gardiner et al., 2000; Peltola et al., 1999), and WINDA (Blennow and Sallnäs, 2004). Considering that such approach is computationally expensive and that high-resolution NWP data accurately representing three-dimensional airflow is scarce, the applicability of conventional mechanistic models to windstorms caused by mountain waves presently appears limited. Pending the development of advanced and cost-effective mechanistic modeling techniques that explicitly account for non-horizontal airflow, progress in understanding and predicting forest wind damage under such conditions is likely to come from data-driven frameworks, specifically robust statistical or machine learning models trained on high-resolution meteorological and forest data.

5. Conclusion

Using the November 2021 mountain wave event in southeastern Norway as a case study, this research highlights the critical role of meteorological variables related to atmospheric stratification, turbulence, and non-horizontal airflow in explaining forest wind damage during mountain wave events. While wind gust speed remains relevant, its explanatory power is limited compared to atmospheric variables, such as the potential temperature gradient and vertical air velocity. We found that forest stand properties, including dominant height (*OH*), diameter at breast height (*DBH8*), and crown coverage (*CC*), did not significantly contribute to explaining the observed damage patterns.

These findings suggest that, in mountain wave events, damage patterns are primarily influenced by localized turbulence and variations in vertical airflow, factors not accounted for by conventional mechanistic wind damage models. Although the November 2021 case study offers strong empirical support, further research is needed to examine whether these processes dominate in other windstorms in complex terrain.

Future studies should apply similar methodologies to windstorm events to validate our findings and explore whether high-resolution atmospheric modelling can improve the representation of wind damage probability in mountain landscapes, including windstorms unrelated to mountain waves.

Funding

This work was in part supported by the Research Council of Norway under Grant 301745 as part of the MARCSMAN (Maximizing the Resilience and Carbon Sequestration in Managed Norway Spruce Forests) project.

CRediT authorship contribution statement

Peter Zubkov: Writing – original draft, Visualization, Validation, Methodology, Investigation, Formal analysis, Data curation. **Harold McInnes:** Writing – review & editing, Methodology, Visualization, Funding acquisition. **Eirik Mikal Samuelsen:** Writing – review & editing, Visualization, Software, Methodology, Investigation. **Kristina Blennow:** Writing – original draft, Writing – review & editing, Supervision, Methodology, Funding acquisition, Conceptualization.

Declaration of competing interest

The authors declare the following financial interests/personal relationships which may be considered as potential competing interests:

Kristina Blennow reports financial support was provided by Research Council of Norway. If there are other authors, they declare that they have no known competing financial interests or personal relationships that could have appeared to influence the work reported in this paper.

Acknowledgements

The authors are grateful to Skogbrand Forsikringsselskap Gjensidig for making available their forest windthrow damage observations collected after the windstorm of 19 November 2021 and to the two anonymous reviewers who helped us significantly improve this paper.

Data availability

I have shared information and links in the manuscript file

References

Albrecht, A., Hanewinkel, M., Bauhus, J., Kohnle, U., 2012. How does silviculture affect storm damage in forests of south-western Germany? Results from empirical modeling based on long-term observations. Eur J Res 131 (1), 229–247.

Anselin, L., 1995. Local Indicators of Spatial Association—LISA. Geogr Anal 27 (2), 93–115.

Armi, L., Mayr, G.J., 2007. Continuously stratified flows across an Alpine crest with a pass: shallow and deep föhn. Q. J. R. Meteorol. Soc. 133 (623), 459–477.

Aune, B., Harstveit, K., 1992. The Storm of 1 January 1992. Meteorological Institute, Norway. Report No. 23/92.

Bénard, P., et al., 2010. Dynamical kernel of the Aladin–NH spectral limited-area model: revised formulation and sensitivity experiments. Q. J. R. Meteorol. Soc.: j. atmos. sci. appl. meteorol. phys. oceanogr. 136 (646), 155–169.
Bengtsson, L., et al., 2017. The HARMONIE–AROME Model Configuration in the ALADIN–HIRLAM NWP System. Mon. Weather Rev. 145 (5), 1919–1935.
Blennow, K., Andersson, M., Sallnäs, O., Olofsson, E., 2010. Climate change and the probability of wind damage in two Swedish forests. For, Ecol, Manage 259 (4), 818–830.
Blennow, K., Olofsson, E., 2008. The probability of wind damage in forestry under a changed wind climate. Clim Change 87 (3), 347–360.
Blennow, K., Persson, E., et al., 2013. Societal Impacts of Storm Damage. Editors. In: Gardiner, B., et al. (Eds.), Living With Storm Damage to Forests. What Science Can Tell Us 3. European Forest Institute.
Blennow, K., Sallnäs, O., 2004. WINDA—A system of models for assessing the probability of wind damage to forest stands within a landscape. Ecol Modell 175 (1), 87–99.
Breiman, L., 2001. Random Forests. Mach Learn 45 (1), 5–32.
Chen, Y.-Y., et al., 2018. Simulating damage for wind storms in the land surface model ORCHIDEE-CAN (revision 4262). Geosci. Model Dev. 11 (2), 771–791.
Cheung, H.M., Chu, J.-E., 2023. Global increase in destructive potential of extratropical transition events in response to greenhouse warming. npj Clim. Atmos. Sci. 6 (1).
Díaz-Yáñez, O., Mola-Yudego, B., González-Olabarria, J.R., 2019. Modelling damage occurrence by snow and wind in forest ecosystems. Ecol Modell 408, 108741.
Dupont, S., Pivato, D., Brunet, Y., 2015. Wind damage propagation in forests. Agric Meteorol 214-215, 243–251.
Durran, D.R., et al., 1990. Mountain Waves and Downslope Winds. Editors. In: Banta, R. M., et al. (Eds.), Atmospheric Processes over Complex Terrain. American Meteorological Society, Boston, MA, pp. 59–81.
ESRI, 2024. ArcGIS Pro v. 3.2. Redlands. Environmental Systems Research Institute, CA.
Feser, F., et al., 2015. Storminess over the North Atlantic and northwestern Europe—A review. Q. J. R. Meteorol. Soc. 141 (687), 350–382.
Frogner, I.-L., Singleton, A.T., Køltzow, M.Ø., Andrae, U., 2019. Convection-permitting ensembles: challenges related to their design and use. Q. J. R. Meteorol. Soc. 145 (S1), 90–106.
Gardiner, B., 2021. Wind damage to forests and trees: a review with an emphasis on planted and managed forests. J. For. Res. 26 (4), 248–266.
Gardiner, B., et al., 2010. Destructive Storms in European Forests: Past and Forthcoming Impacts. Final report to European Commission - DG Environment, Joensuu, Finland.
Gardiner, B., Marshall, B., Achim, A., Belcher, R., Wood, C., 2005. The stability of different silvicultural systems: a wind-tunnel investigation. For.: Int. J. For. Res. 78 (5), 471–484.
Gardiner, B., Peltola, H., Kellomäki, S., 2000. Comparison of two models for predicting the critical wind speeds required to damage coniferous trees. Ecol Modell 129 (1), 1–23.
Gregow, H., Rantanen, M., Laurila, T.K., Mäkelä, A., 2020. Review On winds, Extratropical Cyclones and Their Impacts in Northern Europe and Finland. Reports 2020:3. Finnish Meteorological Institute, Helsinki, Finland.
Groenemeijer, P., et al., 2016. Present and Future Probability of Meteorological and Hydrological Hazards in Europe. ESSL, Delft. Technical Report. Report number: 608166-D 2.5.
Grønås, S., Sandvik, A.D., 1999. Numerical simulations of local winds over steep orography in the storm over north Norway on October 12, 1996. J. Geophys. Res.: Atmos. 104 (D8), 9107–9120.
Hale, S.E., et al., 2015. Comparison and validation of three versions of a forest wind risk model. Environ. Model. Softw. 68, 27–41.
Hanewinkel, M., 2005. Neural networks for assessing the risk of windthrow on the forest division level: a case study in southwest Germany. Eur J Res 124 (3), 243–249.
Hanewinkel, M., Kuhn, T., Bugmann, H., Lanz, A., Brang, P., 2014. Vulnerability of uneven-aged forests to storm damage. Forestry 87 (4), 525–534.
Hanewinkel, M., Peyron, J.L., et al., 2013. The Economic Impact of Storms. Editors. In: Gardiner, B., et al. (Eds.), Living With Storm Damage to Forests. What Science Can Tell Us 3. European Forest Institute.
Hanewinkel, M., Zhou, W., Schill, C., 2004. A neural network approach to identify forest stands susceptible to wind damage. For, Ecol, Manage 196 (2), 227–243.
Harstveit, K., Andresen, L., Midtbø, K., 1995. Downslope Windstorms At Oppdal, Norway. Local description and Numerical Simulations. Norwegian Meteorological Institute. Report No. 23/95.
Hart, E., et al., 2019. Use of machine learning techniques to model wind damage to forests. Agric Meteorol 265, 16–29.
Ikonen, V.-P., et al., 2017. Regional risks of wind damage in boreal forests under changing management and climate projections. Can. J. For. Res. 47 (12), 1632–1645.
Intergovernmental Panel on Climate Change (IPCC), 2023. Weather and Climate Extreme Events in a Changing Climate, Climate Change 2021 – The Physical Science Basis: Working Group I Contribution to the Sixth Assessment Report of the Intergovernmental Panel On Climate Change. Cambridge University Press, pp. 1513–1766.
Jackson, P.L., Mayr, G., Vosper, S., 2013. Dynamically-Driven Winds. Editors. In: Chow, F.K., De Wekker, S.F.J., Snyder, B.J. (Eds.), Mountain Weather Research and Forecasting: Recent Progress and Current Challenges. Springer Netherlands, Dordrecht, pp. 121–218.
Jung, C., Lackmann, G.M., 2023. Changes in Tropical Cyclones Undergoing Extratropical Transition in a Warming Climate: quasi-Idealized Numerical Experiments of North Atlantic Landfalling Events. Geophys Res Lett 50 (8).
Kamimura, K., et al., 2022. Tree dynamic response and survival in a category-5 tropical cyclone: the case of super typhoon Trami. Sci Adv 8 (10), eabm7891.
Kjellström, E., et al., 2018. European climate change at global mean temperature increases of 1.5 and 2 °C above pre-industrial conditions as simulated by the EURO-CORDEX regional climate models. Earth Syst. Dyn. 9 (2), 459–478.
Komonen, A., Schroeder, L.M., Weslien, J., 2011. Ips typographus population development after a severe storm in a nature reserve in southern Sweden. J. Appl. Entomol. 135 (1–2), 132–141.
Kurbatova, M., Rubinstein, K., Gubenko, I., Kurbatov, G., 2018. Comparison of seven wind gust parameterizations over the European part of Russia. Adv, Sci, Res 15, 251–255.
Lenderink, G., Holtslag, A.A.M., 2004. An updated length-scale formulation for turbulent mixing in clear and cloudy boundary layers. Q. J. R. Meteorol. Soc. 130 (604), 3405–3427.
Lilly, D.K., Klemp, J.B., 1979. The effects of terrain shape on nonlinear hydrostatic mountain waves. J Fluid Mech 95 (2), 241–261.
Locatelli, T., Tarantola, S., Gardiner, B., Patenaude, G., 2017. Variance-based sensitivity analysis of a wind risk model - Model behaviour and lessons for forest modelling. Environ. Model. Softw. 87, 84–109.
Lundberg, S.M., Lee, S.-I., 2017. A unified approach to interpreting model predictions. In: Proceedings of the 31st International Conference on Neural Information Processing Systems. Curran Associates Inc., Long Beach, California, USA, pp. 4768–4777.
Lundberg, S.M., et al., 2018. Explainable machine-learning predictions for the prevention of hypoxaemia during surgery. Nat. Biomed. Eng. 2 (10), 749–760.
Mass, C.F., Conrick, R., Weber, N., Zagrodnik, J.P., 2019. The Quinault Blowdown: a Microscale Wind Event Driven by a Mountain-Wave Rotor. Bull. Am. Meteorol. Soc. 100 (6), 977–986.
Masson, V., et al., 2013. The SURFEXv7.2 land and ocean surface platform for coupled or offline simulation of earth surface variables and fluxes. Geosci, Model Dev 6 (4), 929–960.
Meyers, M.P., Snook, J.S., Wesley, D.A., Poulos, G.S., 2003. A Rocky Mountain Storm. Part II: the Forest Blowdown over the West Slope of the Northern Colorado Mountains—Observations. Anal. Model., Weather Forecast. 18 (4), 662–674.
Moran, P.A.P., 1950. Notes on Continuous Stochastic Phenomena. Biometrika 37 (1/2), 17–23.
Müller, M., et al., 2017. AROME-MetCoOp: A Nordic Convective-Scale Operational Weather Prediction Model, 32. Weather and Forecasting, pp. 609–627.
NIBIO, 2024. SR16 - The Norwegian Forest Resource Map.
Økland, B., Berryman, A., 2004. Resource dynamic plays a key role in regional fluctuations of the spruce bark beetles Ips typographus. Agric, For, Entomol 6 (2), 141–146.
Patacca, M., et al., 2023. Significant increase in natural disturbance impacts on European forests since 1950. Glob Chang Biol 29 (5), 1359–1376.
Pawlik, Ł., Harrison, S.P., 2022. Modelling and Prediction of Wind Damage in Forest Ecosystems of the Sudety Mountains, 815. SW Poland. Science of The Total Environment, 151972.
Pedregosa, F., et al., 2011. Scikit-learn: machine Learning in Python. J. Mach, Learn, Res 12, 2825–2830.
Peltola, H., Kellomäki, S., Väisänen, H., Ikonen, V.-P., 1999. A mechanistic model for assessing the risk of wind and snow damage to single trees and stands of Scots pine, Norway spruce, and birch. Can. J. For. Res. 29 (6), 647–661.
Pettit, J.L., et al., 2021. Both Cyclone-induced and Convective Storms Drive Disturbance Patterns in European Primary Beech Forests. J. Geophys. Res.: Atmos. 126 (7).
Poëtte, C., et al., 2017. The Impact of Landscape Fragmentation on Atmospheric Flow: a Wind-Tunnel Study. Bound. Layer Meteorol 163 (3), 393–421.
Queney, P., Corby, G., Gerbier, N., Koschmieder, H., Zierep, J., 1960. The airflow over mountains. World Meteorol. Organ. Tech, Note 34.
Quine, C.P., Gardiner, B.A., Moore, J., 2021. Chapter 4. Wind disturbance in forests: the process of wind created gaps, tree overturning, and stem breakage. Editors. In: Johnson, E.A., Miyanishi, K. (Eds.), Plant Disturbance Ecology (Second Edition). Academic Press, San Diego, pp. 117–184.
Reed, W.J., 1984. The effects of the risk of fire on the optimal rotation of a forest. J Env. Econ Manage 11 (2), 180–190.
Rieutord, T., Bessardon, G., Gleeson, E., 2024. High-Resolution Land Use Land Cover Dataset for Meteorological Modelling—Part 2: ECOCLIMAP-SG-ML an Ensemble Land Cover Map. Land (Basel) 13 (11), 1875.
Romagnoli, F., et al., 2023. Windstorm impacts on European forest-related systems: an interdisciplinary perspective. For, Ecol, Manage 541, 121048.
Ruosteenoja, K., Vihma, T., Venäläinen, A., 2019. Projected Changes in European and North Atlantic Seasonal Wind Climate Derived from CMIP5 Simulations. J Clim 32 (19), 6467–6490.
Saarinen, N., et al., 2016. Using multi-source data to map and model the predisposition of forests to wind disturbance. Scand. J. For. Res. 31 (1), 66–79.
Samuelsen, E., Kvist, K., 2024. Icing Observed and Analysed in Correspondence with Helicopter Flight Campaigns in Norway in 2023. In: Proceedings of the 20th International Workshop on Atmospheric Icing of Structures. IWAIS, 2024.
Sandvik, A.D., Harstveit, K., 2005. Study of a Down Slope Windstorm Over Southern Norway. Norwegian Meteorological Institute, Rjukan, 16 January 2000. Report no. 18/05.
Schelhaas, M.-J., Nabuurs, G.-J., Schuck, A., 2003. Natural disturbances in the European forests in the 19th and 20th centuries. Glob Chang Biol 9 (11), 1620–1633.
Schindler, D., Jung, C., Buchholz, A., 2016. Using highly resolved maximum gust speed as predictor for forest storm damage caused by the high-impact winter storm Lothar in Southwest Germany. Atmos. Sci. Lett. 17 (8), 462–469.
Schwarzbauer, P., Rauch, P., et al., 2013. Impact on Industry and Markets - Roundwood Prices and Procurement Risks. Editors. In: Gardiner, B., et al. (Eds.), Living With Storm Damage to Forests. What Science Can Tell Us 3. European Forest Institute.

Shapley, L.S., 1953. A Value for n-Person Games. Editors. In: Harold William, K., Albert William, T. (Eds.), Contributions to the Theory of Games, Volume II. Princeton University Press, Princeton, pp. 307–318.
Skattør, H.B., Mamen, J., Mjelstad, H., Berger, A.C., Walløe, T.A., 2021. Hendelsesrapport 25/2021: Svært kraftige Vindkast i Agder og På Østlandet fredag 19. November 2021. MET-info, Oslo. Meteorologisk institutt.
Skogbrand Forsikringsselskap Gjensidig, 2022a. Forsikringsvilkår av 1. mars 2022. Skogbrand Forsikringsselskap Gjensidig.
Skogbrand Forsikringsselskap Gjensidig, 2022b. Skadet volum etter stormen 19.11.2021 og stormene i januar-februar 2022. Skogbrand Forsikringsselskap Gjensidig.
Suvanto, S., Peltoniemi, M., Tuominen, S., Strandström, M., Lehtonen, A., 2019. High-resolution mapping of forest vulnerability to wind for disturbance-aware forestry. For, Ecol, Manage 453, 117619.
Valinger, E., Fridman, J., 2011. Factors affecting the probability of windthrow at stand level as a result of Gudrun winter storm in southern Sweden. For, Ecol, Manage 262 (3), 398–403.
Valkonen, T., et al., 2020. Evaluation of a sub-kilometre NWP system in an Arctic fjord-valley system in winter. Tellus A: Dyn. Meteorol. Oceanogr. 72 (1), 1838181.
Venäläinen, A., et al., 2004. Simulations of the influence of forest management on wind climate on a regional scale. Agric Meteorol 123 (3), 149–158.
Viken Skog, 2021. Store skogskader i flere områder.
Wagner, J., et al., 2017. Observed versus simulated mountain waves over Scandinavia – improvement of vertical winds, energy and momentum fluxes by enhanced model resolution? Atmos. Chem. Phys. 17 (6), 4031–4052.
Zimová, S., Dobor, L., Hlásny, T., Rammer, W., Seidl, R., 2020. Reducing rotation age to address increasing disturbances in Central Europe: potential and limitations. For, Ecol, Manage 475, 118408.
Zubkov, P., et al., 2024. Predicting snow damage in conifer forests using a mechanistic snow damage model and high-resolution snow accumulation data. Scand. J. For. Res. 39 (1), 59–75.
Zubkov, P., Solberg, S., Mcinnes, H., 2023. Windthrow damage detection in Nordic forests by 3D reconstruction of very high-resolution stereo optical satellite imagery. Int J Remote Sens 44 (16), 4963–4988.